



HAL
open science

Software for CT-image Analysis to Assist the Choice of Mechanical-ventilation Settings in Acute Respiratory Distress Syndrome

E.E. Dávila Serrano, François Dhelt, Laurent Bitker, Jean-Christophe Richard, Maciej Orkisz

► **To cite this version:**

E.E. Dávila Serrano, François Dhelt, Laurent Bitker, Jean-Christophe Richard, Maciej Orkisz. Software for CT-image Analysis to Assist the Choice of Mechanical-ventilation Settings in Acute Respiratory Distress Syndrome. 2020 International Conference on Computer Vision and Graphics (ICCVG 2020), Sep 2020, Varsovie, Poland. 10.1007/978-3-030-59006-2_5 . hal-02887264

HAL Id: hal-02887264

<https://hal.science/hal-02887264>

Submitted on 14 Dec 2022

HAL is a multi-disciplinary open access archive for the deposit and dissemination of scientific research documents, whether they are published or not. The documents may come from teaching and research institutions in France or abroad, or from public or private research centers.

L'archive ouverte pluridisciplinaire **HAL**, est destinée au dépôt et à la diffusion de documents scientifiques de niveau recherche, publiés ou non, émanant des établissements d'enseignement et de recherche français ou étrangers, des laboratoires publics ou privés.

Software for CT-image analysis to assist the choice of mechanical-ventilation settings in acute respiratory distress syndrome^{*}

Eduardo E. Dávila Serrano¹[0000-0001-5480-5769], François Dhelft^{1,2}[0000-0002-2920-9831], Laurent Bitker^{1,2}[0000-0002-4698-053X], Jean-Christophe Richard^{1,2}[0000-0003-1503-3035], and Maciej Orkisz¹[0000-0003-1709-5766]

¹ Univ Lyon, Université Claude Bernard Lyon 1, INSA-Lyon, UJM-Saint Etienne, CNRS, Inserm, CREATIS UMR 5220, U1206, F-69621, Lyon, France
{davila,jean-christophe.richard,maciej.orkisz}@creatis.insa-lyon.fr
<https://www.creatis.insa-lyon.fr/site7/en>

² Service de Réanimation Médicale, Hôpital de la Croix Rousse, Hospices Civils de Lyon, France
{francois.dhelft,laurent.bitker,j-christophe.richard}@chu-lyon.fr

Abstract. Acute respiratory distress syndrome (ARDS) is a critical impairment of the lung function, which occurs – among others – in severe cases of patients with Covid-19. Its therapeutic management is based on mechanical ventilation, but this may aggravate the patient’s condition if the settings are not adapted to the actual lung state. Computed tomography images allow for assessing the lung ventilation with fine spatial resolution, but their quantitative analysis is hampered by the contrast loss due to the disease. This article describes software developed to assist the clinicians in this analysis by implementing semi-automatic algorithms as well as interactive tools. The focus is the assessment of the cyclic hyperinflation, which may lead to ventilator-induced lung injury. For this purpose aerated parts of the lungs were segmented in twenty ARDS patients, half with Covid-19. The results were in very good agreement with manual segmentation performed by experts: 5.3% (5.1 ml) mean difference in measured cyclic hyperinflation.

Keywords: Acute respiratory distress syndrome · Hyperinflation · Lung segmentation. · Computed tomography · Thoracic images

1 Introduction

Acute respiratory distress syndrome (ARDS) is a particularly severe impairment of the lung function resulting in a very high mortality. Its therapeutic management is based on mechanical ventilation with positive end-expiratory pressure

^{*} This work was performed within the framework of the LABEX PRIMES (ANR-11-LABX-0063) of Université de Lyon, within the program “Investissements d’Avenir” (ANR-11-IDEX-0007) operated by the French National Research Agency (ANR).

(PEEP) used in an attempt to control hypoxemia and hypercapnia, and thus keep the patient alive during the treatment of the syndrome’s actual cause. Nevertheless, experimental and clinical studies have repeatedly demonstrated that inadequate ventilator settings are likely to aggravate ARDS lung injury [9]. Customizing these settings requires quantitative assessment of each patient’s lung response to mechanical ventilation.

Thoracic computed tomography (CT) is the reference technique for quantifying pulmonary aeration in vivo [2] provided that the lungs are delineated from the surrounding tissues. Unfortunately, while segmenting healthy lungs in CT scans is eased by high contrast between the lung parenchyma and other tissues, the segmentation of diseased lungs remains challenging [7]. In particular, the radiological hallmark of ARDS is the presence of large heterogeneous non-aerated (opaque) regions (Fig.1), which defeat the existing segmentation methods and require human interaction to improve results. Literature on automatic lung segmentation for ARDS is very limited. Recently published methods obtained promising results, but were designed for animal models of the syndrome [8,4]. For these reasons, as well as due to the lack of dedicated software, CT is still not used in clinical practice to assist the physicians in setting the main ventilation parameters: PEEP and tidal volume (VT).

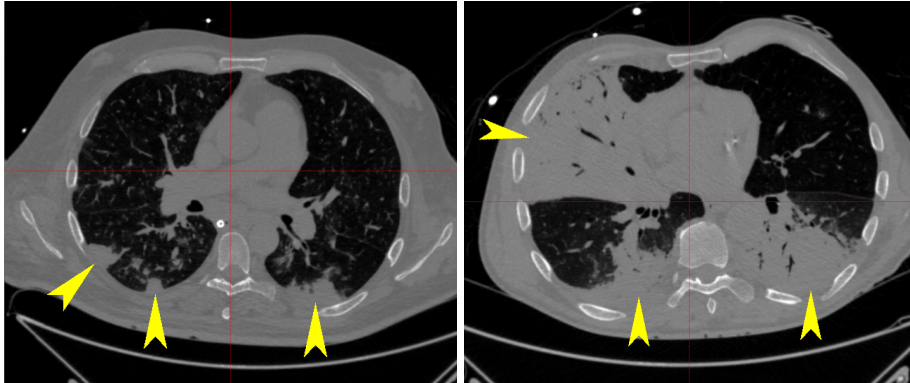


Fig. 1. Examples of slices from thoracic CT scans of patients with mild (left) and severe (right) ARDS. Arrows indicate opaque regions that cannot be distinguished from the surrounding tissues based on gray-levels.

To address the clinicians’ needs we developed a software designed for quantitative analysis of CT-scan pairs acquired at end-inspiration (referred to as *inspi*) and end-expiration (*exp*i**). The project described in this article specifically tackles the assessment of cyclic hyperinflation, i.e., locally excessive lung inflation at each insufflation from the ventilator, which probably reflects too large tidal volume and may lead to ventilator-induced lung injury (VILI). This task requires the segmentation of two three-dimensional (3D) CT images, each of the order of

512³ voxels with sub-millimeter spatial resolution. To be usable in the clinical practice, the whole process – from image loading to numerical result display – must hold within a few minutes.

To achieve these objectives, a dedicated graphical user interface (GUI) implements a series of relatively simple algorithms, mainly based on seeded region growing and mathematical morphology, as well as smart interactive tools allowing the user to quickly edit the result if necessary. Although none of these components is novel, their assembly constitutes a new software that fills the void and finally makes it possible to provide decision support within a time-frame compatible with clinical practice. Herein, we will first describe the main components, then preliminary results on twenty ARDS patients will be reported.

2 Method

Figure 2 displays the main functions available via the GUI of the software, which is helpful to summarize the workflow. The left panel encapsulates *inspi* and *expi* image anonymization, loading, and visual inspection, as well as manual entry of data missing in the DICOM header, such as PEEP, VT, and patient’s height. The right panel contains the whole processing pipeline from an interactive selection of a seed point to data exportation toward a secured-access database. Let us note, that each step can be repeated, if necessary, after visual inspection of the results. As the data can be pushed onto the database at any stage of the process, the completeness of the process needs to be controlled via the **summary** that gives access to a table specifying the already performed steps with their date and hour, as well as to the database itself via a web-page. The subsequent sections will describe in details the segmentation and interactive-correction steps.

2.1 Segmentation

As this work deals with the aerated part of the lungs, like in [5], let us specify the relationship between aeration and CT-image gray levels, actually CT-numbers in

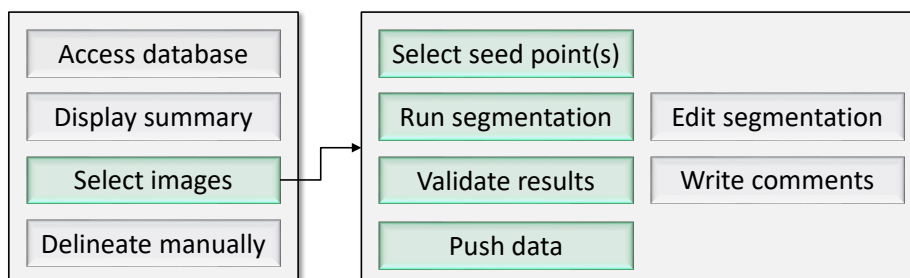


Fig. 2. Main functions available via the graphical user interface. Mandatory operations are highlighted by color. **Run segmentation** and **Edit segmentation** steps are respectively described in Sections 2.1 and 2.2.

Hounsfield units (HU). This relationship is almost linear for lung tissues, where $I_{air} \leq I(\mathbf{x}) \leq I_{water}$, so that air fraction in a voxel \mathbf{x} is calculated as [10]:

$$a(\mathbf{x}) = \frac{I_{water} - I(\mathbf{x})}{I_{water} - I_{air}}, \quad (1)$$

with $I_{air} = -1000$ HU corresponding to pure air and $I_{water} = 0$ HU corresponding to air-free parenchymal tissue (alveolar walls, capillary blood vessels, etc.). In normal parenchyma, air fraction is comprised between 50 and 90%, i.e., $I(\mathbf{x}) \in [-900, -500]$ HU. Above 90% ($I(\mathbf{x}) < -900$ HU) the lung tissue is considered as hyperinflated, between 50% and 10%, i.e., $I(\mathbf{x}) \in [-500, -100]$ HU, as poorly aerated, and below 10% ($I(\mathbf{x}) \geq -100$ HU) as non-aerated [3]. In healthy lungs the hyperinflated interval, which is the focus of our study, is only observed in large airways, but it can also be encountered in the stomach, in the esophagus, and obviously outside the patient’s body.

In mechanically ventilated lungs, hyperinflated regions may occur at any location; therefore, our approach consists in segmenting out the aerated region ($I(\mathbf{x}) < -100$ HU) connected to the trachea (see flowchart Fig. 3), and then quantifying its sub-regions that meet the criterion $I(\mathbf{x}) < -900$ HU, regardless their connectivity. Hence, the initial segmentation is based on region-growing that starts from a seed placed by the user in the trachea, and stops when no more connected voxels below the threshold $I_{th1} = -100$ HU can be added to the region. If visual inspection of the result detects large aerated regions disconnected from the trachea (typically by a mucus plug in a bronchus), additional seeds may be interactively selected and the segmentation may be re-run.

Unfortunately, density intervals of various tissues overlap, and fat contained within the rib-cage muscles may fall below I_{th1} , which results in segmentation leaks between ribs towards subcutaneous fat and even out of the body. To break these leaks, morphological erosion is performed using a structuring element of 3^3 voxels and the number of iterations empirically set to two, and then the lung region is selected by morphological reconstruction using the seed(s) as a marker.

We have observed that, in very fat patients, leaks were too large, erosion with $n = 2$ iterations was not sufficient to break them, while increasing n excessively

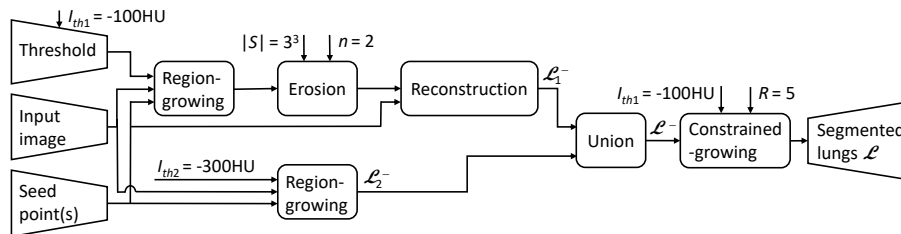


Fig. 3. Segmentation flowchart. Inputs in trapezes are selected by the user; the other parameters were preset: default thresholds $I_{th1} = -100$ HU and $I_{th2} = -300$ HU, structuring-element size $|S| = 3^3$, number of iterations $n = 2$, and ball radius $R = 5$ for the constrained region-growing.

altered the shape of the segmented region. Instead of seeking a complicated automatic solution, we implemented a simple interactive “little help”: the user can use a slider to lower the threshold I_{th1} , and then restart the process. The segmentation result obtained to this point will be referred to as \mathcal{L}_1^- regardless the threshold value used (default $I_{th1} = -100$ HU or manually adjusted).

Erosion not only breaks leaks and “peels” the lung surface; it also removes thin regions within the lungs, namely small bronchi surrounded by non-aerated parenchyma. As long as these are connected to main airways, they can be recovered by an additional region-growing from the same seed(s) as the previous one, but using a threshold empirically set to $I_{th2} = -300$ HU, so as to penetrate far enough into the small bronchi, while avoiding leaks. The regions \mathcal{L}_2^- thus segmented are then added to the previous ones: $\mathcal{L}^- = \mathcal{L}_1^- \cup \mathcal{L}_2^-$.

The last step aims at recovering the outer layer of lung voxels (with densities below I_{th1}) “peeled” by erosion, as well as airway voxels with densities between -300 and -100 HU left out by the conservative stopping criterion of the second region-growing. To this purpose, a spatially-constrained region-growing operator is used. Similar to “onion-kernel” growing [6], this ball-shaped operator starts the growth from its center and agglomerates all connected voxels such that $I(\mathbf{x}) < I_{th1}$, as long as they are located within the ball. This operator is successively placed on each surface-point of \mathcal{L}^- , and its radius is calculated as $R = 2n + 1$.

2.2 Correction

The segmentation process described in the previous section may miss isolated regions. As such regions may also be located outside of the lungs, e.g., in the esophagus, fat, etc., we leave the last word to the human expert who can edit the segmentation result using smart tools specifically adapted for this task. The main goal is to aggregate missing voxels \mathbf{x} that meet the criterion $I(\mathbf{x}) < I_{th1}$. To this purpose, two similar ball-shaped tools are available.

- **fill**: This tool uses the spatially-constrained region-growing operator described in the previous section, which adds voxels meeting this criterion within the ball, only if they are connected to the user-selected ball center.
- **brush**: This tool adds all the voxels meeting the criterion within the ball, regardless their connectivity.

For both tools, the user can select the radius of the ball and choose between its application in 3D or 2D. In the latter case, the tools may be applied in axial, coronal, or sagittal planes, according to the user’s choice.

In some cases, it may also be useful to erase some excess voxels included in the segmentation result \mathcal{L} . This can be done using a ball-shaped eraser, the size of which can also be selected by the user. Obviously, to cope with possible user mistakes, we have implemented an undo/redo button.

2.3 Implementation

The software was implemented using the CreaTools³ framework [1], which builds on well-known free open-source libraries (itk, vtk, wxWidgets), and significantly speeds-up the development of medical image-analysis applications. The database was built using Girder⁴ web-based platform, which also is free and open source.

Figure 4 displays the GUI page corresponding to the **Validate results** function (see Fig. 2). In this example, the lung volume undergoing the cyclic hyperinflation was as large as 45% of the tidal volume (VT). The 3D segmentation results are superimposed onto the original images in axial, sagittal, and coronal views. The sliders can be used to adjust the opacity of the segmentation results, thus showing or hiding the underlying gray-level image. The user can explore any cross-section by moving a cross-hair, and the image contrast can be adjusted using the mouse buttons. After validation, the numerical results displayed in the lower panel are exported to a text file compatible with spread-sheets.

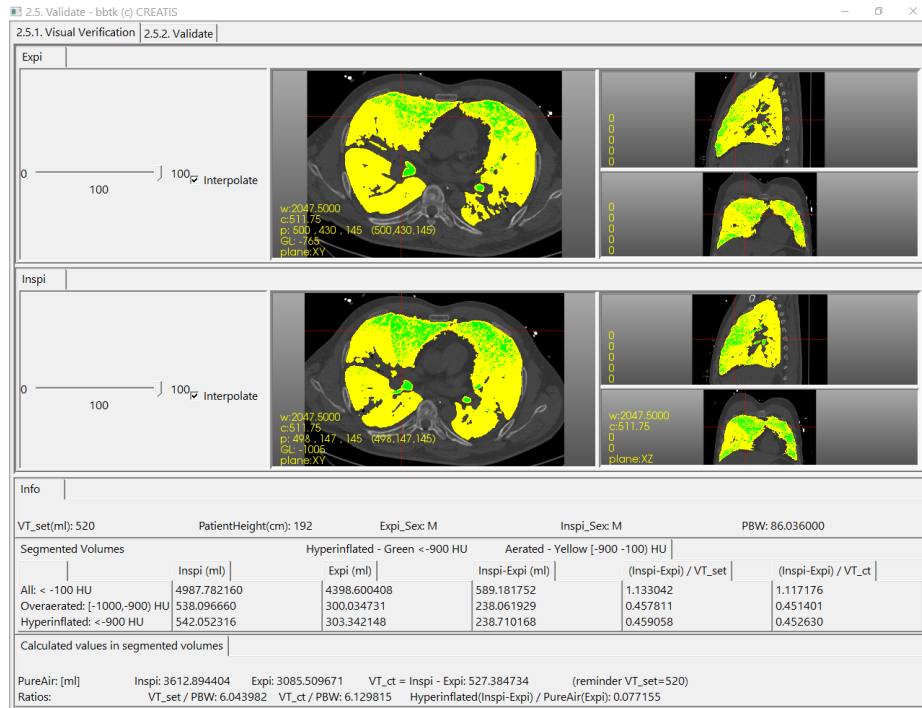


Fig. 4. Example of results submitted to user validation. Yellow color represents the segmentation of all aerated regions, while green color highlights the hyperinflated subregions in *expi* (upper panel) and *inspi* (central panel) images.

³ https://www.creatis.insa-lyon.fr/site7/en/CreaTools_home

⁴ <https://girder.readthedocs.io>

3 Experiments and results

Our software is being evaluated within a prospective study on ARDS patients from the intensive care unit of the La Croix-Rousse Hospital, Lyon France. Hereafter, we will summarize the results obtained on data from the first twenty patients, half of them being diagnosed as Covid-19 positives. There are two 3D CT images (*inspi* and *expi*) for each patient, so the segmentation results reported correspond to forty 3D images each one containing a number of slices ranging from 238 to 384, with slice thickness of 1 mm, in-plane dimensions of 512×512 pixels, and in-plane resolution ranging from 0.57×0.57 to 0.88×0.88 mm.

For the purpose of this evaluation, each patient’s complete lungs are manually segmented in both *inspi* and *expi* images. The segmentation is made “from scratch” by a medical expert blinded to the results of the semi-automatic segmentation, who uses an interactive segmentation program specially developed for this task and available from the main GUI (function `Delineate manually` in Figure 2). Let us note that this program allowed a significant reduction of operating time, as compared to general-purpose medical-image segmentation software: from six hours to 1.5 hour to delineate the lungs in a pair of CT scans. The reference segmentation thus obtained is then subdivided into non-aerated, poorly aerated, normally aerated and hyperinflated compartments by use of the standard thresholds: -100 , -500 , and -900 HU (see Section 2.1). The aerated sub-regions (compartments below -100 HU) are then compared with their counterpart in the semi-automatic segmentation results. It is important to note that the experts delineate only the lungs, without large airways (trachea and main bronchi), whereas the semi-automatic segmentation includes the latter.

All results reported hereafter were obtained with minimum interaction, i.e., with a single seed point per 3D CT scan and no manual correction. Voxels present in both manual and semi-automatic segmentation results are called true positives. Voxels present in the manual segmentation result but not in the semi-automatic one are called false negatives. Similarly, voxels present in the semi-automatic segmentation result, but not in the manual one are called false positives. The number of voxels in the respective categories is referred to as TP , FN , and FP . In Table 1, these values are reported as volumes, i.e., after multiplying by voxel size. They were used to calculate performance indexes: Dice score (also known as F-measure) $Dice = 2TP / (2TP + FP + FN)$, recall (also

Table 1. Mean values of TP , FP , and FN volumes expressed in milliliters, followed by mean values \pm standard deviations of Dice score, recall, and precision. The last two columns contain Dice score and precision values calculated from \overline{TP} , \overline{FP} , and \overline{FN} .

Compartment	\overline{TP}	\overline{FP}	\overline{FN}	$Dice$	Rec	$Prec$	$Dice_{tot}$	$Prec_{tot}$
Hyperinflated	190.5	27.2	0.0	0.66 ± 0.27	1.00 ± 0.00	0.55 ± 0.29	0.94	0.89
Normally aerated	1969.9	16.8	2.5	0.99 ± 0.01	1.00 ± 0.01	0.99 ± 0.00	1.00	0.99
Poorly aerated	803.2	41.4	65.0	0.94 ± 0.05	0.94 ± 0.10	0.95 ± 0.03	0.93	0.95
All aerated	2963.6	85.4	67.5	0.97 ± 0.03	0.97 ± 0.06	0.97 ± 0.01	0.97	0.97

Table 2. Mean volume changes between *inspi* and *expi* scans: M stands for the results calculated from manual segmentation, S for semi-automatic, $D = S - M$, and $L = TP + FN$ is the aerated lung volume from manual segmentation of the *expi* scan.

Compartment	S [ml]	M [ml]	D [ml]	D/M	D/L
Hyperinflated	101.1	96.0	5.1	5.3%	0.2%
Normally aerated	406.3	403.7	2.7	0.7%	0.2%
Poorly aerated	-29.8	-51.2	21.5	-41.9%	1.2%
All aerated	477.7	448.5	29.2	6.5%	1.5%

known as sensitivity or true-positive rate) $Rec = TP / (TP + FN)$, and precision $Prec = TP / (TP + FP)$.

Table 2 reports the mean values of volume changes between the same patient’s *inspi* and *expi* scans, calculated from manual (M) and semi-automatic (S) segmentation results. Like in the previous table, these are displayed for all compartments, as well as for the entire segmented regions (last line). These volume changes reflect the distribution of the air supplied by ventilator. In both semi-automatic and manually-obtained results, it can be seen that, while the total increase in aerated volume was – on average – below 500 ml, approximately 100 ml of this increase affected the hyperinflated compartment. Let us recall, that this corresponds to the undesired cyclic hyperinflation. Conversely, the increase in the normally-aerated volume is an expected effect, although the most desirable effect is the decrease in poorly- and non-aerated volumes, which become normally- and poorly-aerated, respectively. Unfortunately, the decrease in poorly-aerated volume was much smaller than the increase in hyperinflated volume, which may mean that VT was sometimes excessive. When comparing the semi-automatic and manually-obtained results, it can be observed that the largest difference ($D = S - M$) corresponds to the poorly-aerated compartment, which is the least contrasted with respect to the surrounding tissues, and thus the most difficult to segment. Nevertheless, although this difference was large compared to the volume change in this compartment, it remained very limited (1.2%) in comparison with the total volume of the aerated lung tissues (L).

A more precise assessment of air distribution in different compartments requires the use of Equation 1 to calculate the quantity of air in each voxel. By summing up the contributions of each voxel, we compared the *inspi-to-expi* change in air quantities calculated within the segmented lungs, and the VT values set on the ventilator. The difference was equal to -1.5% on average, which is much less than the uncertainty of this setting on the ventilator (assessed by means of a calibrating device), and tends to confirm the accuracy of our segmentation.

The processing time was measured on a PC with Intel(R) Core(TM) i7-6820HQ CPU @ 2.70GHz 8 processors and 16 GB memory. The automatic segmentation of one average-size (317 slices) 3D CT image took 46 seconds (except interactive selection of the seed point) and required 2.7 GB of memory. Approximately 75% of this time was spent on the constrained region-growing process. The total execution time of the application `Run segmentation`, i.e., loading in-

put files for the selected patient, segmenting both *inspi* and *expi* 3D CT scans, and writing output files, was of 109 seconds.

4 Discussion and conclusion

The focus of this study is the cyclic hyperinflation of the lungs. The proposed software was able to accurately calculate this value with user interaction limited to one click within the trachea. The mean disagreement with respect to the results obtained manually was of 5.1 ml, which represents 5.3% of the measured value. The volume of false positives in Table 1 suggests that semi-automatic segmentation tends to overestimate the aerated volume. This can be easily explained for the hyperinflated and normally-aerated compartments: whereas trachea and main bronchi were included in the semi-automatic segmentation, they were excluded from the manual one. This is not a problem in our application, where only the difference between *inspi* and *expi* volumes is of interest. Indeed, the walls of the trachea and main bronchi are quite rigid (cartilageous), so the encompassed sub-volume remains unchanged and subtraction cancels its contribution. If necessary, a strategy to remove the extra sub-volume can be implemented. Nevertheless, false positives due to the inclusion of trachea and main bronchi considerably decreased the Dice score and precision for segmentation results in the hyperinflated compartment in cases where the true volume of this compartment was close to zero. This is reflected by low mean values and large standard deviations. For this reason, we also reported the indexes $Dice_{tot}$ and $Prec_{tot}$ calculated from the mean values of TP , FP , and FN . These show that the overall agreement with manual segmentation was good in all compartments.

Please note that the volume of false negatives in hyperinflated and normally aerated compartments was close to zero, which means that almost no voxels were missed. Larger false-negative volumes (comparable with false positives) were observed only in the poorly-aerated compartment. As image contrasts between these regions and the extra-pulmonary tissues are considerably decreased, both semi-automatic and manual delineation of their outer boundary is more difficult. Therefore, the quality of the semi-automatic segmentation may be poorer, but the reliability of the manual reference may also be questioned.

Although validation of the proposed software is still ongoing on a larger cohort of patients, the preliminary results reported in this article are very promising, and the clinicians have begun to use it for the purpose of comparison between ARDS patients diagnosed with Covid-19 and those without the virus. The algorithms implemented in the software do not attempt to delineate the non-aerated regions, and state-of-the-art methods also fail to satisfactorily perform this task [5]. Our current investigation aims at overcoming this limitation, as quantifying the *expi-to-inspi* changes in this compartment would allow the assessment of another important ventilatory parameter: the alveolar recruitment.

In conclusion, so far analyzed results on 20 ARDS patients show that the proposed software meets the clinicians' expectations in terms of processing time, accuracy, and user-friendly interactive tools. For the first time, CT scans can be

used to calculate the lung volume subjected to cyclic hyperinflation within a few minutes. The underlying semi-automatic segmentation can be performed by a non-expert medical operator. The next step is to integrate this tool into a real-time ventilator-adjustment strategy.

References

1. Dávila Serrano, E.E., Guigues, L., Roux, J.P., Cervenansky, F., Camarasu-Pop, S., Riveros Reyes, J.G., Flórez-Valencia, L., Hernández Hoyos, M., Orkisz, M.: CreaTools: A framework to develop medical image processing software: Application to simulate pipeline stent deployment in intracranial vessels with aneurysms. In: Bolc, L., Tadeusiewicz, R., Chmielewski, L., Wojciechowski, K. (eds.) *Computer Vision and Graphics, ICCVG 2012, Lecture Notes in Computer Science*, vol. 7594, pp. 55–62. Springer Berlin Heidelberg (2012). https://doi.org/10.1007/978-3-642-33564-8_7
2. Gattinoni, L., Caironi, P., Pelosi, P., Goodman, L.R.: What has computed tomography taught us about the acute respiratory distress syndrome? *Am J Respir Crit Care Med* **164**(9), 1701–11. (Nov 2001). <https://doi.org/10.1164/ajrccm.164.9.2103121>
3. Gattinoni, L., Caironi, P., Cressoni, M., Chiumello, D., Ranieri, V.M., Quintel, M., Russo, S., Patroniti, N., Cornejo, R., Bagedo, G.: Lung recruitment in patients with the acute respiratory distress syndrome. *New England Journal of Medicine* **354**(17), 1775–1786 (apr 2006). <https://doi.org/10.1056/nejmoa052052>
4. Gerard, S.E., Herrmann, J., Kaczka, D.W., Musch, G., Fernandez-Bustamante, A., Reinhardt, J.M.: Multi-resolution convolutional neural networks for fully automated segmentation of acutely injured lungs in multiple species. *Medical Image Analysis* p. 101592 (2019). <https://doi.org/10.1016/j.media.2019.101592>
5. Klapsing, P., Herrmann, P., Quintel, M., Moerer, O.: Automatic quantitative computed tomography segmentation and analysis of aerated lung volumes in acute respiratory distress syndrome - a comparative diagnostic study. *Journal of Critical Care* **42**, 184–191 (dec 2017). <https://doi.org/10.1016/j.jcrc.2016.11.001>
6. Lidayová, K., Gómez Betancur, D.A., Frimmel, H., Hernández Hoyos, M., Orkisz, M., Smedby, Ö.: Airway-tree segmentation in subjects with acute respiratory distress syndrome. In: *Image Analysis*, pp. 76–87. Springer International Publishing (Lidayova2017). https://doi.org/10.1007/978-3-319-59129-2_7
7. Mansoor, A., Bagci, U., Foster, B., Xu, Z., Papadakis, G.Z., Folio, L.R., Udupa, J.K., Mollura, D.J.: Segmentation and image analysis of abnormal lungs at CT: Current approaches, challenges, and future trends. *RadioGraphics* **35**(4), 1056–1076 (jul 2015). <https://doi.org/10.1148/rg.2015140232>
8. Morales Pinzón, A., Orkisz, M., Richard, J.C., Hernández Hoyos, M.: Lung segmentation by cascade registration. *IRBM* **38**(5), 266–280 (oct 2017). <https://doi.org/10.1016/j.irbm.2017.07.003>
9. Nieman, G.F., Satalin, J., Andrews, P., Aiash, H., Habashi, N.M., Gatto, L.A.: Personalizing mechanical ventilation according to physiologic parameters to stabilize alveoli and minimize ventilator induced lung injury (vili). *Intensive Care Medicine Experimental* **5**(1), 8 (Feb 2017). <https://doi.org/10.1186/s40635-017-0121-x>
10. Yin, Y., Hoffman, E.A., Lin, C.L.: Mass preserving nonrigid registration of CT lung images using cubic B-spline. *Medical Physics* **36**(9), 4213–4222 (2009). <https://doi.org/10.1118/1.3193526>